ORIGINAL PAPER

# Establishing conditions for simulating hydrophobic solutes in electric fields by molecular dynamics

## Effects of the long-range van der Waals treatment on the apparent particle mobility

**Zoran Miličević · Siewert J. Marrink · Ana-Sunčana Smith · David M. Smith**

**Abstract** Despite considerable effort over the last decade, the interactions between solutes and solvents in the presence of electric fields have not yet been fully understood. A very useful manner in which to study these systems is through the application of molecular dynamics (MD) simulations. However, a number of MD studies have shown a tremendous sensitivity of the migration rate of a hydrophobic solute to the treatment of the long range part of the van der Waals interactions. While the origin of this sensitivity was never explained, the mobility is currently regarded as an artifact of an improper simulation setup. We explain the spread in observed mobilites by performing extensive molecular dynamics simulations using the GROMACS software package on a system consisting of a model hydrophobic object (Lennard-Jones particle) immersed in water both in the presence and absence of a static electric field. We retrieve a unidirectional field-induced mobility of the hydrophobic object when the forces are simply truncated. Careful analysis of the data shows that, only in the specific case of truncated forces, a non-zero van der Waals force acts, on average, on the Lennard-Jones particle. Using the Stokes law we demonstrate that this force yields quantitative agreement with the field-induced mobility found within this setup. In contrast, when the treatment of forces is continuous, no net force is observed. In this manner, we provide a simple explanation for the previously controversial reports.

**Keywords** Molecular dynamics · Electrophoretic mobility · Van der Waals interactions · GROMACS

This paper belongs to a Topical Collection on the occasion of Prof. Tim Clark's 65th birthday

Z. Miličević · A.-S. Smith (✉) · D. M. Smith (✉)
Cluster of Excellence: Engineering of Advanced Materials, Friedrich-Alexander University Erlangen-Nuremberg, Nägelsbachstraße 49b, 91052 Erlangen, Germany
e-mail: smith@physik.fau.de
e-mail: dsmith@irb.hr

Z. Miličević · A.-S. Smith
Institute for Theoretical Physics, Friedrich-Alexander University Erlangen-Nuremberg, Staudtstraße 7, 91058 Erlangen, Germany

A.-S. Smith · D. M. Smith
Ruđer Bošković Institute, Bijenička cesta 54, 10000 Zagreb, Croatia

S. J. Marrink
Groningen Biomolecular Sciences and Biotechnology Institute and Zernike Institute for Advanced Materials, University of Groningen, Nijenborgh 7, 9747AG Groningen, The Netherlands

## Introduction

The hydrophobicity of an interface, droplet or a particle can be modulated by an external electric field in a process called electrowetting [1]. Such a change of surface characteristics allows for the regulation of macroscopic properties such as adhesion or friction in micro and nano-fluidics by the electric field [2]. Microfluidic movement [3] based on electrowetting is being used in an increasing number of applications, for example, for reflective displays [4, 5]. While the effect of the electric field is reasonably well understood on the macroscopic scale [1], there are only a few studies of the origin of electrowetting on the nanometric scale [6–8]. With the advent of nano-electronics and the development of micro and nano-devices that can be powered by electric fields [9], this becomes an increasingly pressing problem.

In the presence of a static electric field, it has been found that the field exerts torques on non-spherical nano-particles [10]. This occurs through a coupling between the interfacial hydrogen bonds and the alignment of the water molecules, which has also been studied in the context of nanodrops on graphene surfaces [11] and for water in nanopores [6, 12]. It is natural to expect that this coupling will also affect the hydration of spherical nano-particles, and thus have implications on the self-assembly process, the propulsive efficiency of nano-devices, and the electrophoretic mobility [13] of particles.

Recently, an interesting coupling between the electric field and the solvent organization was suggested, supposedly leading to net water flux through carbon nanotubes in the presence of static fields. The latter were directly imposed [14] or mimicked by an asymmetric distribution of point charges along the tube [15], while the van der Waals (vdW) forces were truncated after a certain cutoff distance. However, in both cases, the flux was found to vanish when the van der Waals interactions were gradually turned off [16, 17]. Additionally, the flux was found to be somewhat sensitive to the neighbor list update frequency, the commonly used Berendsen thermostat, as well as to the improper use of the charge groups [17, 18]. However, since the strongest effect was associated with the treatment of the long range vdW interactions, the mobility observed with the truncated forces was argued to be the consequence of the imprudent implementation of the Lennard-Jones cut scheme within GROMACS [16, 18, 19].

Similar arguments were evoked after the electrophoretic mobility of heptane droplets in ion-free water in the presence of static external fields was reported as a result of an MD study, again using GROMACS [20]. The mobility was initially related to the interfacial water structure, involving static properties such as the water dipolar ordering and the density profile as well as dynamic properties such as the viscosity and the slip length [21]. The mechanism was later disputed by Bonthuis et al [19], who showed that in an electroneutral dipolar fluid the static electric fields do not give rise to interfacial flow, even in the presence of dipolar ordering at the surface. Their conclusion was supported by the observation that the mobility indeed vanishes when the long-ranged van der Waals interactions are treated by the shift approach instead of the default cut(off) approach. Even though the correctness of the GROMACS package was questioned several times, quantitative explanation of such tremendous sensitivity of the nano-fluidic mobility on the treatment of the van der Waals interactions and on other simulation parameters has not yet been presented.

In this work we attempt to explain this sensitivity by constructing a minimal model that could show mobility. More specifically, as shown in Fig. 1, we perform extensive MD simulations in GROMACS of a perfectly spherical
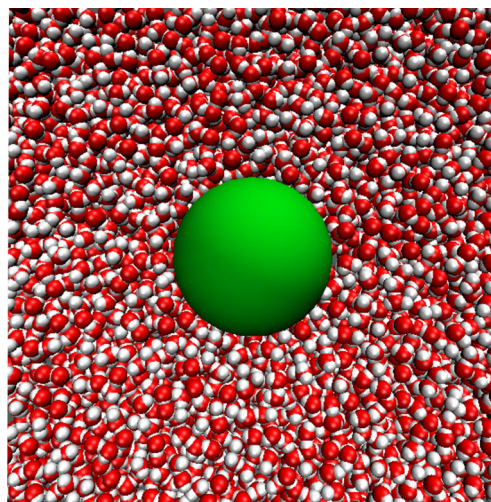


**Fig. 1** A snapshot from the simulation of a Lennard-Jones particle (*large green sphere*) immersed in water

hydrophobic particle in water, both in the presence and absence of an external electric field.

## Methods

### Computational details

The standard simulation setup involves a single uncharged Lennard-Jones (LJ) sphere, with a mass of 50 atomic mass units and the van der Waals interaction parameters $\sigma_{LJ-O}$ and $\varepsilon_{LJ-O}$ of 1.5 nm and 0.8063 kJ mol$^{-1}$, respectively. These were deliberately set to create a particle that is significantly larger than the water molecule (Fig. 1). The particle was dissolved in a cubic box of edge length 8.9 nm containing 23419 SPC/E [22] water molecules. The energy of the system was first minimized with the steepest descent method. Subsequently, a short (0.5-1 ns, NPT) run was performed followed by an additional equilibration run (0.5-1 ns, NPT) at nonzero field for the simulations in the presence of an external electric field. The latter was chosen to have a strength of 0.6 V nm$^{-1}$, and was imposed using tinfoil boundary conditions [23]. During the equilibration, the pressure was weakly coupled to a target value of $p = 1$ bar using the Berendsen barostat [24]. In all cases, the volume of the system fully relaxed and began to fluctuate around an equilibrium value.

The production runs (each with a total length of 100 ns) were conducted in both the NVT and the NPT ensembles, in the presence and absence of a static electric field (imposed in the $+x$ direction). For the simulations in the NVT ensemble, the initial 0.5-1 ns was omitted from the analysis, to allow the relaxation of the system after fixing its volume, i.e. density. For all combinations of the ensemble

and field strength, the simulations were performed for the three common treatments of the van der Waals interactions, namely the cut, switch, and shift treatments.

The standard setup involved simulations with a time step of 2 fs, the LINCS algorithm [25], particle decomposition, and a non-bonded list update frequency (NLUF) of 10 steps. Long range electrostatic interactions were accounted for by the Particle Mesh Ewald (PME) [26] technique. A reference temperature of 300 K was achieved by employing the Berendsen algorithm with a time relaxation constant of 0.1 ps [24]. To ensure good statistics and adequate spatial and time resolution, the coordinates were saved, with single precision, every 100 steps. To evaluate the results, single precision simulations (forces, velocities, and positions) were compared to runs subject to double precision evaluations (through all levels of the simulation).

Unless indicated otherwise, simulations were performed in the GROMACS 4.0.5 simulation package [27]. Additional simulations were executed in GROMACS 3.3.3, 4.5.5, and 4.6.4.

In the study of the effect of the thermostat (NVT ensemble, NLUF=1, and NLUF=10), the standard Berendsen weak coupling scheme was replaced with the Nosé-Hoover [28, 29] thermostat (with a period of oscillations of kinetic energy set to 0.3 ps), or the advanced velocity rescaling [30] algorithm (relaxation time of 0.1 ps), as implemented in the 4.0.5 version of GROMACS. In addition, Langevin thermostat (friction constant 0.5 ps$^{-1}$) was implemented together with the Langevin dynamics [31].
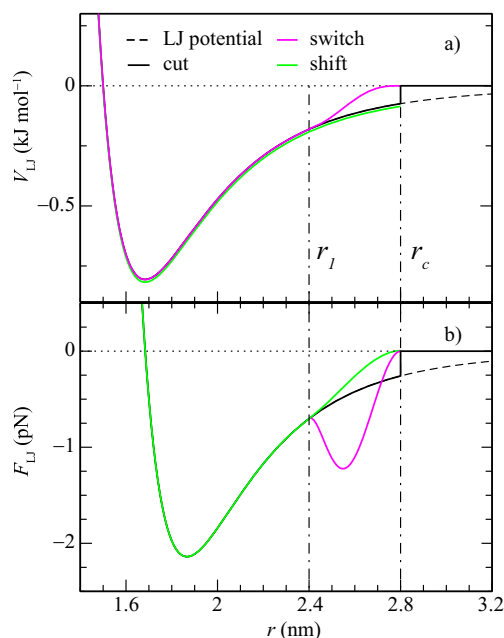
Treatments of the van der Waals interactions

Generally, van der Waals interactions are taken into account through the well known 12-6 Lennard-Jones potential (dashed line in Fig. 2a)

$$V_{\text{LJ}} = 4\varepsilon_{ij} \left[ \left( \frac{\sigma_{ij}}{r_{ij}} \right)^{12} - \left( \frac{\sigma_{ij}}{r_{ij}} \right)^{6} \right], \qquad (1)$$

where $\varepsilon_{ij}$ is the potential well depth and $\sigma_{ij}$ is the distance between atoms $i$ and $j$ at which $V_{\text{LJ}} = 0$.

An important characteristic of the LJ potential (1) is its slowly varying dispersion term, that makes the potential long-ranged. To make computation feasible, the most common way is to neglect all interactions between atoms at distances larger than the chosen cutoff distance $r_c$. This is referred to as the *cut* treatment. While computationally very effective, this treatment has a discontinuity both in the potential and in the force at the cutoff distance (black lines in Fig. 2).

Because we here focus on the nonbonded interactions of the LJ particle with water, the cutoff distance is chosen relatively large. More specifically, we explicitly take into



**Fig. 2** The potential (**a**) and the force (**b**) for the cut (*black lines*), switch (*purple lines*) and shift (*green lines*) treatments of the van der Waals interactions between the oxygen atom of a water molecule and the LJ particle, when $\sigma_{\text{LJ-O}} = 1.5$ nm, $\varepsilon_{\text{LJ-O}} = 0.8063$ kJ mol$^{-1}$. The *dot-dashed lines* indicate the boundaries of the transition region, namely $r_1 = 2.4$ nm and the cutoff radius $r_c = 2.8$ nm

account the interaction of the LJ particle with at least the 4 nearest layers of water

$$r_c \gtrsim \sigma_{\text{LJ-O}} + 4\sigma_{\text{H}_2\text{O}} , \qquad (2)$$

where $\sigma_{\text{H}_2\text{O}} = 0.31$ nm. Hence, the cutoff radius is rounded to 2.8 nm.

In order to replace the truncated potentials by continuous ones that also have continuous derivatives, other treatments of the vdW potential have been proposed [32, 34, 35]. In the context of the GROMACS package, two such treatments are extensively used. The first is called *shift* [34] and it introduces a function which modifies the potential over its whole range ($0 \leq r < r_c$). The second is called *switch* and modifies the potential over part of the range ($r_1 \leq r < r_c$). Fundamentally, there is no difference between the switch and shift treatments since for $r_1 = 0$ the latter reduces to the former one. The region $r_1 \leq r < r_c$, which shows the largest deviations of the potential and/or force from the original, will be referred to as the transition range.

Within the switch treatment (purple lines in Fig. 2), the LJ interaction potential (1) is multiplied by a switch function $S(r)$ defined as

$$S(r) = \begin{cases} 1, & \text{if } r \leq r_1 \\ 1 - 10W^3 + 15W^4 - 6W^5, & \text{if } r_1 < r < r_c \\ 0, & \text{if } r \geq r_c \end{cases} \qquad (3)$$

where $W = (r - r_1)/(r_c - r_1)$. This multiplication drives the potential function towards zero at the cutoff distance. The van der Waals force in the switch method reads

$$\mathbf{F}^{sw}(r) = -\nabla(V_{LJ}S) = \mathbf{F}_{LJ}S(r) - V_{LJ}\nabla S(r) , \qquad (4)$$

with $\mathbf{F}_{LJ} = -\nabla V_{LJ}(r)$. The first derivative of the switch function $\nabla S(r)$, and hence the contribution to the total force, is nonzero only in the transition region. Here, the force $\mathbf{F}^{sw}(r)$ gains an additional and spurious second minimum (purple line in Fig. 2b), consequences of which will become evident at a later stage.

In the shift treatment (green lines in Fig. 2) a function is added to the LJ potential [32, 34]

$$V^{sh}(r) = V_{LJ}(r) - V_{LJ}^c + 4\varepsilon_{ij}\left[\sigma_{ij}^{12}A^{rep} - \sigma_{ij}^6 A^{dis}\right] + V_d^{sh}(r). \qquad (5)$$

Here, $V_{LJ}^c$ is the value of the LJ potential at the cutoff distance $r_c$, while $A^{rep}$ and $A^{dis}$ are the repulsion and dispersion corrections of the LJ potential depending only on the values of $r_1$ and $r_c$. The term $V_d^{sh}$ is nonvanishing only for $r_1 < r < r_c$ and equals

$$
\begin{aligned}
V_d^{sh}(r) = & -\frac{4}{3}\varepsilon_{ij}\left(\sigma_{ij}^{12}K_1^{rep} + \sigma_{ij}^6 K_1^{dis}\right)(r - r_1)^3 \\
& -\varepsilon_{ij}\left(\sigma_{ij}^{12}K_2^{rep} + \sigma_{ij}^6 K_2^{dis}\right)(r - r_1)^4 ,
\end{aligned}
\qquad (6)
$$

where $K_1^{rep}$, $K_1^{dis}$, $K_2^{rep}$ and $K_2^{dis}$ are constants depending only on the values of $r_1$ and $r_c$ and the nature of the interaction, i.e. repulsive or attractive (see Supporting Information for full expressions). The resulting potential $V^{sh}(r)$ deviates only slightly from $V_{LJ}(r)$ (green line in Fig. 2a). Importantly, the resulting force $\mathbf{F}^{sh}(r)$ deviates from $\mathbf{F}_{LJ}(r)$ only in the transition region, where it smoothly approaches zero at $r_c$ due to the contribution $\mathbf{F}_d^{sh}(r) = -\nabla V_d^{sh}(r)$ (green line in Fig. 2b).

## Results and discussion

### Water at the interface of the LJ particle

The static structural properties of water around a model hydrophobic object, i.e. the Lennard-Jones particle, can be quantified by the radial distribution function (rdf) between the particle and the oxygen atom of the water molecule $g_{LJ\text{-}O}$ [33, 36–38, 41].

In Fig. 3 we show the rdfs $g_{LJ\text{-}O}$ for all considered treatments of the vdW interactions in the absence of an external electric field. Although we present data obtained in the NVT ensemble, identical results are obtained in the NPT ensemble. The common main features are three well-defined maxima and minima, the latter indicating the edges of the respective hydration shells. Strikingly, a careful inspection
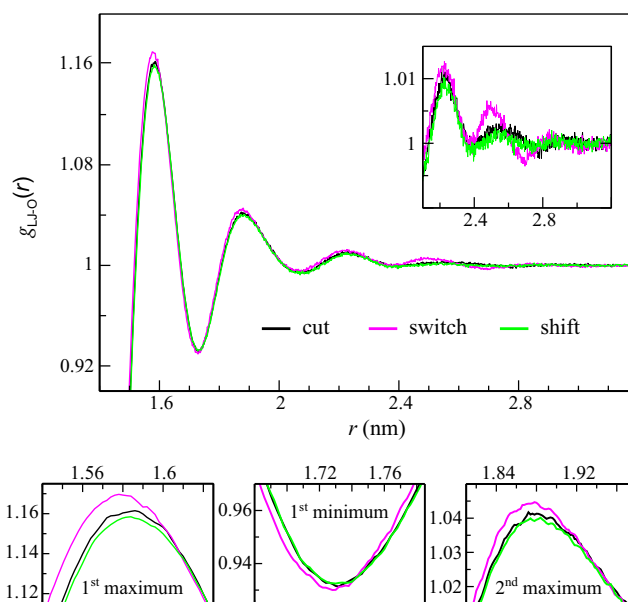


**Fig. 3** Comparison of the radial distribution function $g(r)$ between the LJ particle and water oxygen for the cut, switch and shift treatments of the van der Waals interactions. *Inset* the behavior of $g(r)$ at long distances, $r \geq 2.1$ nm. *Bottom row* the local behavior of $g(r)$ at the positions of 1st and 2nd maxima, and 1st minimum, respectively. The results are for the simulations performed in the NVT ensemble in the absence of an electric field

of the transition region (see inset of Fig. 3) reveals an additional and unexpected structuring in the case of the switch treatment compared to the cut and the shift treatment within the transition region. A clear indication that these correlations, although small, are unphysical is the appearance of more negative correlations ($g < 1$) at the position of the fourth minimum than at the third minimum. Furthermore, even though the vdW force is identical for $r < r_1$ in all three approaches, the perturbation imposed in the transition region propagates towards the hydrophobic object and manifests in subtle changes of water structure closer to the hydrophobic object, as evidenced in the small graphs in the lower row in Fig. 3 representing $g_{LJ\text{-}O}(r)$ around the 1st and 2nd maxima, as well as the 1st minimum. The same increase of correlations observed for the switch treatment in $g_{LJ\text{-}O}$ is apparent in the rdf between the LJ particle and the water hydrogens $g_{LJ\text{-}H}$ (some examples are given in the Supporting Information, Fig. S1a). Furthermore, this increase is independent of the version of GROMACS and the precision at which the simulation is executed.

It is important to stress that similar spurious correlations were not found in any of the water-water rdfs (i.e. $g_{O\text{-}O}$, $g_{H\text{-}H}$, and $g_{O\text{-}H}$), supposedly because the employed cutoffs are too large to have impact on the correlations of the much smaller solvent molecules. However, even with transition regions at much shorter distances ($0.6 - 0.9$ nm, $0.7 - 1.0$ nm, $0.9 - 1.2$ nm, $1.5 - 1.8$ nm), the described increase of

correlations was not found in the rdfs of the water molecules in simulations of a pure water box and the switch treatment. This is presumably because at these distances the dominant interactions between water molecules are of Coulomb type.

In the presence of the electric field, the analysis of the water structure around a hydrophobic object has not yet been performed systematically for different vdW treatments. The difficulty is the breaking of the isotropy due to a specifically imposed field orientation. Consequently, averaging over two spatial coordinates respecting azimuthal symmetry must be performed to fully resolve the distribution of water at the interface. Unfortunately, such an analysis would require sampling statistics that are currently out of reach. We thus analyze the radially averaged distribution function which still contains the relevant information (Fig. S1b). We find that when vdW interactions are treated with the switch function, the same increase of structuring as in the absence of the field can be seen. Such an observation is in agreement with previous results on the treatment of electrostatic interactions with an atom-based switch function [42]. Therein, it was shown that such an electrostatic switch treatment induces artificial dipolar ordering of water in the transition region [35].

It is clear that different treatments of vdW interactions indeed induce subtle changes of the water structure around a hydrophobic object. However, it is not clear if these small differences can be related to the potentially different mobilities of LJ particles in water. To see these effects, we further study the dynamics of the system.

## Observed time-dependent displacement of the LJ particle

We first investigate the time-dependent displacement $\Delta$ of the LJ particle both in the presence and absence of a static electric field (Fig. 4). At zero field, the average displacement, $\langle \Delta \rangle = (\Delta_x + \Delta_y + \Delta_z)/3$, is fully comparable to a trajectory along a particular coordinate. In the presence of the electric field, we focus on the displacement along the $x$ axis which coincides with the direction of the field.

In Fig. 4, we show the results for both the NVT and the NPT ensembles and all three treatments of vdW interactions. Independently of the ensemble, the majority of the displacement curves show a strong resemblance to trajectories expected from a particle exhibiting Brownian motion. The switch treatment provides an analogous behavior to the shift, despite the slight differences in the static organization of interfacial waters. On the time scale of 100 ns, the displacements observed with these two treatments in the presence of the field are indistinguishable from those at zero field. The exception is the superficially small preference to move in a direction opposite to the field, which is an effect that we could not prove to be statistically relevant at this stage. However, a stark contrast can be seen in the displacements under the field when using the truncated vdW forces. These curves show a linear drift superimposed on the Brownian displacement, which is suggestive of a net force acting on the particle. We find field-induced velocities of the LJ particle of $-0.45$ m s$^{-1}$ (NVT) and $-0.41$ m s$^{-1}$ (NPT), obtained from linear fits to the respective data sets (dashed lines).

Comparable velocities were found in several previous studies with the cut treatment [15, 17–19, 21] on similar systems. The latter was declared spurious after no net movement (or water flux) was found on comparable time scales when the shift method was employed with the field [17, 19]. Actually, a non-zero flux of water molecules through a carbon nanotube [18] was observed for the cut treatment even in the absence of the electric field. Since we find no particular displacement of the LJ particle when $E = 0$, the reported flux seems to be related to the particularity of the investigated system.

Apart from the cut-off treatment, other parameters such as the time step, the neighbor list update frequency (NLUF) or the Berendsen thermostat (BT) were suggested to induce unphysical motion of water around a hydrophobic object in GROMACS, although these results were based on relatively short simulations [17]. We test these parameters (BT, NLUF) in a set of 100 ns long simulations (cut treatment, NVT ensemble, and $E_0 = 0.6$ V nm$^{-1}$), and show the results in Fig. 5, alongside the reference setup (BT, NLUF = 10). A constant negative drift velocity is
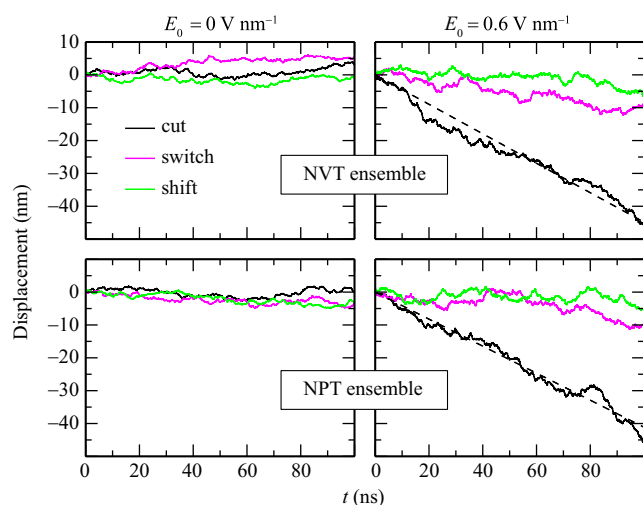
**Fig. 4** The displacement of the LJ particle in the absence (*left*) and the presence of static electric fields (*right*). In the absence of electric fields the average displacement over three Cartesian directions is shown. In the presence of electric fields the displacement in the field direction (imposed in the $+x$ direction) is shown. In the *upper* and *lower row* are data for the NVT and the NPT ensemble, respectively. The total simulation time for each setup is 100 ns. The *dashed black lines* are the linear fits of the displacement to illustrate the unidirectionality of the movement of the Lennard-Jones particle
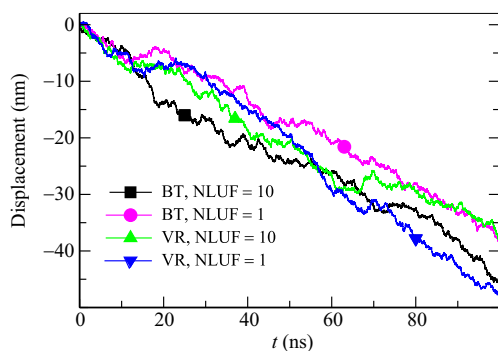
**Fig. 5** The displacement of the LJ particle in the direction of the imposed static electric field, $E_x = 0.6$ V nm$^{-1}$. The simulations are performed in the NVT ensemble and the vdW interactions are represented by the cut scheme. *Legend* BT - Berendsen thermostat, VR - velocity rescale, NLUF - neighbor list update frequency (# timesteps)

observed for each setup, while the difference between the curves is within the expected statistical noise. The insensitivity of the drift motion on the NLUF indicates that the water molecules positioned around $r_c$, that actually contribute to the update of the neighbor list of the LJ particle, do not cause the drift. Thus, the mechanism that drives the net movement of the LJ particle in a direction opposite to the field is most likely related to the solute-solvent interface effects. Additionally, we obtained very similar displacements with the advanced velocity rescaling (VR) algorithm [30] ($-0.39$ m s$^{-1}$ for NLUF = 10 and $-0.46$ m s$^{-1}$ for NLUF = 1) and the Berendsen algorithm ($-0.45$ m s$^{-1}$ for NLUF = 10 and $-0.35$ m s$^{-1}$ for NLUF = 1). Hence, the observed field induced mobility can not be assigned to the imperfections of the Berendsen thermostat, which does not rigorously reproduce a correct thermodynamic ensemble [43].

In addition, we performed simulations of 20 ns, to test the influence of the system size, the time step, and the field strength on the observed magnitude of the field-induced velocity of the LJ particle, in the NVT ensemble using the cut treatment, the Berendsen thermostat, and NLUF = 10. In the system with $N_{H_2O} = 63596$, the observed drift velocity of the LJ particle remained the same as in the smaller system. With the smaller time step the drift was somewhat larger, while with the decrease of the field strength to 0.3 V nm$^{-1}$ the drift was significantly reduced.

Brownian diffusion of the LJ particle

To elucidate the origin of the observed drift, we first analyze the underlying Brownian displacement and determine the diffusion coefficient $D$ of the LJ particle. At zero field, the diffusion coefficient is obtained from the slope of the three dimensional mean square displacement as $D = \langle (\mathbf{r}_{LJ}(t) - \mathbf{r}_{LJ}(0))^2 \rangle / (6t)$, where $\mathbf{r}_{LJ}(t) - \mathbf{r}_{LJ}(0)$ is the distance traveled

by the LJ particle in time $t$. In the presence of the field, we calculate the diffusion coefficient in the field direction as $D_x = \langle (x_{LJ}(t) - x_{LJ}(0))^2 \rangle / (2t)$, where $x_{LJ}(t)$ is the time-dependent position of the LJ particle along the $x$ axis. In order to eliminate effects of the drift, and assure linearity, only the first 50 ps of the mean square displacement curve were used in all cases.

Table 1 summarizes the obtained diffusion coefficients of the LJ particle. At zero field, within the statistical uncertainty, $D$ is found independent of the vdW interaction treatment and the thermodynamic ensemble employed. The same applies in the presence of the electric field with the diffusion coefficient in the field direction possibly slightly enhanced. Similarly, the diffusion coefficient in the directions perpendicular to the field (data not shown) remains unaffected by the treatment of the vdW interactions.

It is worth noting that the measured diffusion coefficients were not sensitive to the version of GROMACS and most of the results fall within the statistical significance of one another. Likewise, the difference between the NVT and NPT ensembles borders with the statistical accuracy. This is presumably the consequence of the employed large system size, when the averages of macroscopic observables become identical in the two ensembles.

The net vdW force on the LJ particle

The linear displacement with the cut approach is indicative of a static net force acting on the particle. As the LJ particle carries no charge, it is difficult to envisage a simple electrostatic force. The only remaining possibility is a force originating in vdW interactions, which is further supported by the sensitivity of the mobility to the vdW treatment. We thus calculate the instantaneous total van der Waals force $\mathbf{F}^{vdW}(t)$ in each Cartesian direction exerted on the LJ particle by the solvent, by adding the contributions from all

**Table 1** The diffusion coefficients (in $10^{-6}$ cm$^2$ s$^{-1}$) of the Lennard-Jones particle for different treatments of the vdW interactions in the presence and absence of electric fields for both the NVT and NPT ensembles. In the presence of the field, the diffusion coefficient in the direction of the field is presented

| Treatment | $E_0$ (V nm$^{-1}$) | NVT | NPT |
|-----------|---------------------|-----|-----|
| CUT | | $2.64 \pm 0.06$ | $2.58 \pm 0.01$ |
| SWITCH | 0.0 | $2.61 \pm 0.03$ | $2.66 \pm 0.05$ |
| SHIFT | | $2.64 \pm 0.03$ | $2.58 \pm 0.01$ |
| | | | |
| CUT | | $2.70 \pm 0.05$ | $2.87 \pm 0.05$ |
| SWITCH | 0.6 | $2.64 \pm 0.01$ | $2.67 \pm 0.01$ |
| SHIFT | | $2.62 \pm 0.05$ | $2.64 \pm 0.03$ |

water molecules found within $r_c$. The net vdW force is taken to be the time average of instantaneous forces

$$\left\langle F_i^{\mathrm{vdW}} \right\rangle = \frac{1}{T} \sum_{j=1}^{T} \sum_{k=1}^{N_w} F_i^{\mathrm{vdW}}(\mathbf{r}_{kj}; r_{kj} < r_c), \quad i \equiv \{x, y, z\}$$

$$(7)$$

where $T$ is the total number of frames (system configurations) analyzed and equals 500 000 in each case, $N_w$ is the total number of water molecules present in the system, and $\mathbf{r}_{kj}$ is the relative position of the oxygen atom (position of the vdW interaction site) of water molecule $k$ with respect to the position of the LJ particle at time frame $j$. The specificity of the van der Waals treatment (cut, switch, shift) employed in each particular setup is taken into account by using an appropriate expression for the force.

Table 2 shows the calculated net vdW forces in each Cartesian direction on the LJ particle. In the absence of the external electric field, independent of the treatment of the vdW interactions and the thermodynamic ensemble, the net force in each Cartesian direction is effectively zero. This is consistent with the observed lack of net drift of the LJ particle. Similarly, with the switch and shift treatment at $E_0 = 0.6$ V nm$^{-1}$ the net force remains effectively zero in all directions, as well as for the cut treatment in the off-field directions.

Strikingly, in the field direction we find a significant net force of $\approx -6.6$ pN acting on the LJ particle. This force is quickly converging and exhibits a standard deviation of about 0.3 pN (see Fig. S2). While this force appears large, it is of a similar magnitude to that exerted by a motor molecule on vesicular cargo. In the aqueous context, this force is about the same as the one acting between the LJ particle and a single water molecule at a distance of about 1.6 nm. Importantly, the magnitude of this force is not related to the version of GROMACS, and is only associated with the cut treatment of the vdW interactions. This is evidenced by the mean force of about $-6.6$ pN determined

in simulations with the standard setup in all studied versions of GROMACS (i.e. 3.3.3, 4.5.5 and 4.6.4). In addition, test simulations performed with double precision did not affect the result. The observed force with the cut treatment was again $-6.5 \pm 0.1$ pN, while the force was vanishing with the shift and switch treatments.

In a more detailed analysis, we find that this force is generated by water molecules belonging to the first two hydration shells while the contribution from waters in the transition region conforms to a Gaussian distribution with zero mean. This is true for all setups, including the ones with the switch treatment.

### Consistency between the evaluated vdW force and the observed drift

If the evaluated force observed with the cut treatment is consistent with the observed drift velocity, the Stokes law should apply

$$\left\langle F_i^{\mathrm{vdW}} \right\rangle = \boldsymbol{\xi}_i \cdot v_i.$$

$$(8)$$

Here $v_i$ is the drift velocity in the direction $i$ of the net force acting on the particle. The proportionality constant $\boldsymbol{\xi}$ is the friction coefficient and is simply related to the diffusion constant by the Einstein relation $\boldsymbol{\xi}_i = k_B T / D_i$ ($k_B$ is the Boltzmann constant).

Using Eq. 8, with $D_x$ from Table 1, and $\langle F_x^{\mathrm{vdW}} \rangle$ from Table 2, for the cut treatment under the field, we predict a drift velocity of $-0.43$ m s$^{-1}$ and $-0.46$ m s$^{-1}$ for the standard setup of parameters in the NVT and the NPT ensemble, respectively. This is in exceptional agreement with the field-induced drift observed in the simulations of $-0.45$ m s$^{-1}$ (NVT) and $-0.41$ m s$^{-1}$ (NPT). The small difference between the predicted and the observed drift velocity can be attributed to the intrinsically present thermal noise resulting from the Brownian motion of the LJ particle. This agreement clearly demonstrates that the observed field-induced mobility of a hydrophobic object is a result of a fluctuating

**Table 2** The net van der Waals force on the Lennard-Jones particle in each Cartesian direction for different treatments of the vdW interactions in the presence and absence of static electric fields imposed in the $+x$ direction

| Treatment | $E_0$ (V nm$^{-1}$) | NVT ensemble | | | NPT ensemble | | |
|---|---|---|---|---|---|---|---|
| | | $\langle F_x^{\mathrm{vdW}} \rangle$ (pN) | $\langle F_y^{\mathrm{vdW}} \rangle$ (pN) | $\langle F_z^{\mathrm{vdW}} \rangle$ (pN) | $\langle F_x^{\mathrm{vdW}} \rangle$ (pN) | $\langle F_y^{\mathrm{vdW}} \rangle$ (pN) | $\langle F_z^{\mathrm{vdW}} \rangle$ (pN) |
| CUT | | $-0.02 \pm 0.07$ | $-0.02 \pm 0.06$ | $0.00 \pm 0.02$ | $-0.01 \pm 0.07$ | $-0.02 \pm 0.10$ | $0.01 \pm 0.05$ |
| SWITCH | 0.0 | $-0.05 \pm 0.06$ | $-0.01 \pm 0.15$ | $0.05 \pm 0.08$ | $0.03 \pm 0.04$ | $0.02 \pm 0.15$ | $0.01 \pm 0.13$ |
| SHIFT | | $-0.02 \pm 0.06$ | $0.00 \pm 0.09$ | $0.01 \pm 0.11$ | $0.01 \pm 0.08$ | $0.07 \pm 0.11$ | $0.00 \pm 0.08$ |
| CUT | | $-6.59 \pm 0.04$ | $0.07 \pm 0.09$ | $0.02 \pm 0.07$ | $-6.62 \pm 0.06$ | $-0.03 \pm 0.15$ | $0.04 \pm 0.11$ |
| SWITCH | 0.6 | $-0.03 \pm 0.09$ | $-0.04 \pm 0.11$ | $0.00 \pm 0.13$ | $0.03 \pm 0.08$ | $-0.02 \pm 0.02$ | $0.05 \pm 0.13$ |
| SHIFT | | $0.03 \pm 0.06$ | $0.01 \pm 0.07$ | $-0.02 \pm 0.08$ | $0.03 \pm 0.05$ | $-0.01 \pm 0.13$ | $0.02 \pm 0.10$ |

but, on average, non-zero force that is produced by truncating the vdW forces. This force is directly related to the field strength, as evidenced by its decrease to $-4.99 \pm 0.03$ pN at the field strength of 0.3 V nm$^{-1}$.

Consistent with the observed drifts discussed in previous sections, we find the average net vdW force on the LJ particle in the field direction for the cut treatment to be independent of the chosen thermostat and NLUF employed. The forces obtained for the test set of simulations in the NVT ensemble (see Fig. 5) are: $-6.7 \pm 0.1$ (VR, NLUF = 10), $-6.61 \pm 0.07$ (VR, NLUF = 1), and $-6.58 \pm 0.05$ pN (BT, NLUF = 1). This is in excellent agreement with $\langle F_x^{\mathrm{cut}} \rangle = -6.59 \pm 0.04$ pN obtained for the standard setup (BT, NLUF = 10). Naturally, the calculated $v_x$ arising from the $\langle F_x^{\mathrm{vdW}} \rangle$ (between $-0.43$ m s$^{-1}$ and $-0.46$ m s$^{-1}$) agrees well with the observed induced field velocities (between $-0.35$ m s$^{-1}$ and $-0.46$ m s$^{-1}$). With the increase of the system size to $N_{\mathrm{H_2O}} = 63596$ we obtain $\langle F_x^{\mathrm{cut}} \rangle = -6.72 \pm 0.03$ pN which is, expectedly, almost the same as in the smaller system. The smaller time step of 1 fs slightly increases the net force to $-7.0 \pm 0.3$ pN, which is in agreement with the somewhat larger drift velocity observed. Since the diffusion coefficient $D_x$ is effectively independent of the simulation setup (data not shown), this data demonstrates that the average net vdW force found on the hydrophobic object is exclusively related to the cut treatment of the vdW interactions.

### The effects of the thermostat and the "flying ice cube" effect

In a number of experimental realizations of electrophoretic experiments, the total number of particles is preserved and the overall system is canonical. Consequently, only the average total energy is preserved. One can introduce this to molecular dynamics by the application of appropriate thermostats, which modify the Newtonian MD scheme such that a statistical ensemble is generated at a constant temperature. However, it is well documented that inappropriate choices of thermostats may significantly affect the fluctuations in the system and, in some cases, induce energy drifts caused by the accumulation of numerical errors [39, 40].

To study these effects in our system, we have performed a set of simulations in a standard setup with different thermostats at 300 K. We sample the instantaneous velocity $v_x$(LJ) along the direction of the imposed field for 10 ns. Since the system is expected to be canonical, this distribution should be a Gaussian identical to the one-dimensional Maxwell-Boltzmann distribution of velocities of a colloid with a mass associated with the LJ particle, generated at 300 K (symbols in Fig. 6a).

Since it is expected that the canonical nature of the system is best reproduced by a Langevin thermostat, we perform Langevin dynamics simulations [31]. In this stochastic but ergodic scheme, each particle is coupled to a local heat bath, which removes heat trapped in localized modes. While the momentum transfer in such simulations is destroyed, making the diffusion coefficients inaccessible with this thermostat, the canonical distribution is obtained accurately, as evidenced in Fig. 6.

In the context of Newtonian dynamics, an attractive and elegant thermostat is that of Nosé-Hoover [28, 29]. It is deterministic, time reversible and in principle canonical (extra degree of freedom acts as thermal reservoir), but sometimes computationally demanding. However, when the system is poorly ergodic, this approach may become difficult and a chain of thermostats may have to be imposed. However, this does not seem to be the case in the current simulations, and an excellent agreement with the canonical
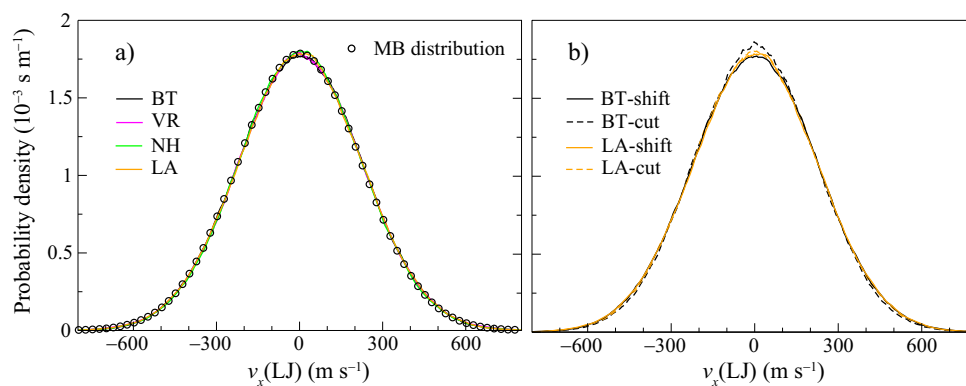


**Fig. 6** (**a**) Comparison of the distribution of the instantaneous velocity (saved at every step for 10 ns) of the LJ particle in the direction of the imposed static electric field, $E_x = 0.6$ V nm$^{-1}$ with the shift treatment. The simulations were performed with the Berendsen thermostat (BT), advanced velocity rescaling (VR), Nosé-Hoover (NH), and by Langevin dynamics (LA). The expected Maxwell-Boltzmann distribution (MB) is shown with symbols. The same analysis for the cut treatment is presented in Fig. S3. (**b**) Comparison of the cut (*dashed lines*) and shift (*full lines*) treatments with the Berendsen (*black*) and the Langevin thermostats (*orange*)

distribution is obtained (Fig. 6a). An equally good agreement with the Maxwell-Bolzmann distribution is obtained with the advanced velocity rescaling method [30], within which the target temperature is drawn from the canonical probability distribution, to produce the correct ensemble.

We compare the performance of these canonical thermostats to the commonly used Berendsen weak coupling scheme [24]. The Berendsen approach gained popularity because of its robustness, speed and easy implementation. The problem with this approach is that it is not time-reversible or deterministic and the resulting distributions do not strictly correspond to any ensemble. In practice, however, the deviations from the canonical distribution are relatively small and decrease with increasing system size. Specifically in our system, the distribution generated with this treatment is within the noise of distributions generated with more formal thermostats for the shift treatment (Fig. 6a). For the cut treatment the Nosé-Hoover, the advanced velocity rescaling and the Berendsen thermostats show small deviations around the maximum from the distribution obtained with the Langevin thermostat, the latter coinciding with the distributions obtained with the shift treatment (Fig. 6b).

The use of the Berendsen thermostat, as well as the imposition of truncation schemes for the vdW forces is sometimes associated with localized and unwanted correlated motions. Spurious drifts may appear due to the transfer of energy from fast to slow degrees of freedom, which is known as the "flying ice cube" effect. There are several steps which help in avoiding this effect, including the use of the here chosen Verlet algorithm to propagate the system. Since this algorithm is time reversible, it is associated with little or no long-term energy drain. Furthermore, it is important to remove all motion of the center of mass of the system (translational and rotational) which we perform in each molecular dynamics step [40]. Beside making relevant choices in setting the simulations, one can test for the "flying ice cube" effect *a posteriori*, by carefully analyzing the entirety of the data, as discussed below.

Several arguments can be used to support our interpretation that the drift velocity is associated with the net force acting on the particle, and not with the "flying ice cube" effect. The first is that the our system reproduces the canonical distribution very well. Its size is such that the thermodynamic limit is approached in the sense that differences between system averages in the NVT and the NPT ensembles are basically within the statistical accuracy. Furthermore, we obtain the same results (net force on the particle as a function of the treatment of the van der Waals forces) independently of the thermostat. Specifically, in a set of 10 ns long simulations, we obtain a net average force in the direction of applied electric field of $-6.7 \pm 0.2$ pN, $-6.5 \pm 0.1$ pN, and $-6.6 \pm 0.3$ pN with the Berendsen, the advanced
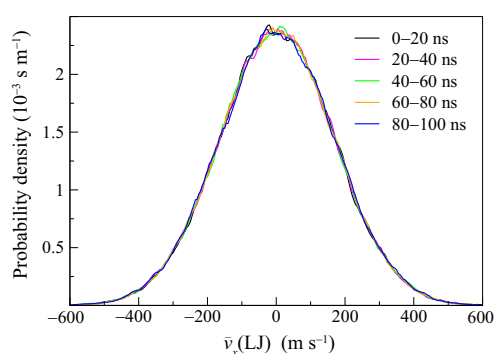


**Fig. 7** The distribution of the velocity of the LJ particle along the direction of the field $\bar{v}_x$(LJ), calculated from the displacement of the LJ particle with the resolution of 0.2 ps. The simulation was performed using the default setup (NVT, BT, NLUF = 10), with the vdW interactions treated using the shift approach. The distribution was generated over 5 successive intervals of 20 ns. The comparison of the results shows no time evolution of the velocity distribution. The same analysis for the cut treatment is presented in Fig. S4

velocity rescaling and the Nosé-Hoover thermostats, respectively. Even the Langevin dynamics yields an average force of $-6.9 \pm 0.3$ pN with the cut treatment. On the other hand the shift treatment always leads to zero force, independently of the thermostat and the integration algorithm. Furthermore, the obtained drift is fully consistent with the observed force, which only occurs with the cut treatment.

While we are able to confidently associate the spurious motion of the LJ particle in the electric field to the cut treatment of the vdW interaction, slow energy transfer could still be possible on even larger time scales. To exclude this, we test for the slow draining of the kinetic energy into the translational degrees of freedom of the particle, by checking its velocity distribution generated in intervals of 20 ns over 100 ns (original protocol, Fig. 7). Here, the velocity was calculated from the actual displacement of the LJ particle with a resolution of 0.2 ps. Importantly, the velocity distribution is fully independent of time, with any of the treatment of the van der Waals interactions (see Fig. 7 for the shift treatment and Fig. S4 for the cut treatment), which we believe, convincingly excludes the existence of drifts associated with "flying ice cube" effect in our simulations.

## Conclusions

Using a series of molecular dynamics simulations in GROMACS, we have investigated the behavior of a solvated nanosized Lennard-Jones particle in the presence of a static electric field, as a function of the treatment of the long-range vdW interactions. Even in the absence of the field, we showed that the different treatments result in subtle changes of the distribution of water molecules at the interface with the LJ particle. These changes are not necessarily correct,

as exemplified by the excessive correlations in the transition region when the switch treatment is used. The observation of a fluctuating but non-zero vdW force on the LJ particle occurring in static electric fields with the cut treatment can be considered in a similar way. Indeed, it is likely that similar forces were responsible for the negative electrophoretic mobilities of hydrophobic objects, and water fluxes through carbon nanotubes, which were reported in previous studies. While the accuracy of GROMACS was brought into question, it seems to be now clear that these effects arise merely from the truncation of the forces, while the spread of the previously reported results may also be associated with the relatively small system sizes and simulation times. This is further supported by the fact, neither the artifacts in the static radial distribution function with the switch treatment, nor the measured forces with the cut treatment depend on the used version of GROMACS. Analogously, the same reasoning can be used to rationalize why the shift implementation for the vdW interactions apparently provides the most accurate results. Despite these clarifications, the subtleties in the organization of water in the first two hydration shells, which give rise to these effects, have yet to be properly characterized.

# References

1. Shamai R, Andelman D, Berge B, Hayes R (2008) Water, electricity, and between . . . On electrowetting and its applications. Soft Matter 4:38–45
2. Robinson L, Hentzell A, Robinson ND, Isaksson J, Berggren M (2006) Electrochemical wettability switches gate aqueous liquids in microfluidic systems. Lab Chip 6:1277–1278
3. Rotenberg B, Pagonabarraga I (2013) Electrokinetics: insights from simulation on the microscopic scale. Mol Phys 111:827–842
4. Hayes RA, Feenstra BJ (2003) Video-speed electronic paper based on electrowetting. Nature 425:383–385
5. Pollack MG, Fair RB, Shenderov AD (2000) Electrowetting-based actuation of liquid droplets for microfluidic applications. Appl Phys Lett 77:1725–1726
6. Bratko D, Daub CD, Luzar A (2009) Water-mediated ordering of nanoparticles in an electric field. Faraday Discuss 141:55–66
7. Dzubiella J, Hansen JP (2005) Electric-field-controlled water and ion permeation of a hydrophobic nanopore. J Chem Phys 122:234,706–14
8. Vaitheeswaran S, Yin H, Rasaiah JC (2005) Water between plates in the presence of an electric field in an open system. J Phys Chem B 109:6629–6635
9. Chang ST, Paunov VN, Petsev DN, Velev OD (2007) Remotely powered self-propelling particles and micropumps based on miniature diodes. Nat Mater 6:235–240
10. Daub CD, Bratko D, Ali T, Luzar A (2009) Microscopic dynamics of the orientation of a hydrated nanoparticle in an electric field. Phys Rev Lett 103:207,801–4
11. Daub CD, Bratko D, Leung K, Luzar A (2007) Electrowetting at the nanoscale. J Phys Chem C 111:505–509
12. Bratko D, Daub CD, Leung K, Luzar A (2007) Effect of field direction on electrowetting in a nanopore. J Am Chem Soc 129:2504–2510
13. O'Brien RW, Beattie JK, Djerdjev AM (2014) The electrophoretic mobility of an uncharged particle. J Colloid Interface Sci 420:70–73
14. Joseph S, Aluru NR (2008) Pumping of confined water in carbon nanotubes by rotation-translation coupling. Phys Rev Lett 101:064,502–4
15. Gong X, Li JY, Lu H, Wan R, Li JC, Hu J, Fang H (2007) A charge-driven molecular water pump. Nat Nanotechnol 2:709–712
16. Bonthuis DJ, Falk K, Kaplan CN, Horinek D, Berker AN, Bocquet L, Netz RR (2010) Comment on Pumping of confined water in carbon nanotubes by rotation-translation coupling. Phys Rev Lett 105:209,401–1
17. Wong-ekkabut J, Miettinen MS, Dias C, Karttunen M (2010) Static charges cannot drive a continuous flow of water molecules through a carbon nanotube. Nat Nanotechnol 5:555–557
18. Bonthuis DJ, Rinne KF, Falk K, Kaplan CN, Horinek D, Berker AN, Bocquet L, Netz RR (2011) Theory and simulations of water flow through carbon nanotubes: prospects and pitfalls. J Phys: Condens Matter 23:184,110–10
19. Bonthuis DJ, Horinek D, Bocquet L, Netz RR (2009) Electrohydraulic power conversion in planar nanochannels. Phys Rev Lett 103:144,503–4
20. Knecht V, Levine ZA, Vernier PT (2010) Electrophoresis of neutral oil in water. J Colloid Interface Sci 352:223–231
21. Knecht V, Risselada HJ, Mark AE, Marrink SJ (2008) Electrophoretic mobility does not always reflect the charge on an oil droplet. J Colloid Interface Sci 318:477–486
22. Berendsen HJC, Grigera JR, Straatsma TP (1987) The missing term in effective pair potentials. J Phys Chem 91:6269–6271
23. Hünenberger P (1999) Simulation and theory of electrostatic interactions in solution: computational chemistry, biophysics, and aqueous solutions. Am Inst Phys:17–83
24. Berendsen HJC, Postma JPM, van Gunsteren WF, DiNola A, Haak JR (1984) Molecular-dynamics with coupling to an external bath. J Chem Phys 81:3684–3690
25. Hess B, Bekker H, Berendsen HJC, Fraaije JGEM (1997) LINCS: A linear constraint solver for molecular simulations. J Comput Chem 18:1463–1472
26. Darden T, York D, Pedersen L (1993) Particle mesh Ewald: An $N \cdot \log(N)$ method for Ewald sums in large systems. J Chem Phys 98:10089–10092
27. van der Spoel D, Lindahl E, Hess B, Groenhof G, Mark AE, Berendsen HJC (2005) Gromacs: Fast, flexible and free. J Comp Chem 26:1701–1718
28. Hoover WG (1985) Canonical dynamics: equilibrium phase-space distributions. Phys Rev A 31:1695–1697
29. Nosé S (1984) A molecular dynamics method for simulations in the canonical ensemble. Mol Phys 52:255–268
30. Bussi G, Donadio D, Parrinello M (2007) Canonical sampling through velocity rescaling. J Chem Phys 126:014,101–7
31. van Gunsteren WF, Berendsen HJC (1988) A leap-frog algorithm for stochastic dynamics. Mol Sim 1:173–185
32. Baron R, Trzesniak D, de Vries AH, Elsener A, Marrink SJ, van Gunsteren WF (2007) Comparison of thermodynamic properties of coarse-grained and atomic-level simulation models. Chem Phys Chem 8:452–461

33. Ashbaugh HS, Paulaitis ME (2001) Effect of solute size and solute-water attractive interactions of hydration water structure around hydrophobic solutes. J Am Chem Soc 123:10721–10728

34. Christen M, Hünenberger P, Bakowies D, Baron R, Bürgi R, Geerke DP, Heinz TN, Kastenholz MA, Kräutler V, Oostenbrink C, Peter C, Trzesniak D, van Gunsteren WF (2005) The GROMOS software for biomolecular simulation: GROMOS05. J Comput Chem 26:1719–1751

35. van der Spoel, D van Maaren PJ (2006) The origin of layer structure artifacts in simulations of liquid water. J Chem Theory Comput 2:1–11

36. Huang DM, Chandler D (2002) The hydrophobic effect and the influence of solute-solvent interactions. J Phys Chem B 106:2047–2053

37. Hummer G, Garde S (1998) Cavity expulsion and weak dewetting of hydrophobic solutes in water. Phys Rev Lett 80:4193–4196

38. Kinoshita M (2005) Density and orientational structure of water around a hydrophobic solute: effects due to the solute size. J Mol Liq 119:47–54

39. Chiu SW, Clark M, Subramaniam S, Jakobsson E (2000) Collective motion artifacts arising in long-duration molecular dynamics simulations. J Comput Chem 21:121–131

40. Harvey SC, Tan RKZ, Cheatham TE (1998) The flying ice cube: velocity rescaling in molecular dynamics leads to violation of energy equipartition. J Comput Chem 19:726–740

41. Smith AS (2005) The total solute-water correlation function forbalancepage Lennard-Jones particles. Fizika A 14:187–194

42. Leach AR (1996) Molecular modelling: principles and applications. Addison-Wesley Longman, Harlow

43. Morishita T (2000) Fluctuation formulas in molecular-dynamics simulations with the weak coupling. J Chem Phys 113(8):2976–2982